

2006

X-Ray Absorption Spectroscopy of the Multiphase Interstellar Medium: Oxygen and Neon Abundances

Y Yao

QD Wang

University of Massachusetts - Amherst

Follow this and additional works at: https://scholarworks.umass.edu/astro_faculty_pubs



Part of the [Astrophysics and Astronomy Commons](#)

Recommended Citation

Yao, Y and Wang, QD, "X-Ray Absorption Spectroscopy of the Multiphase Interstellar Medium: Oxygen and Neon Abundances" (2006). *The Astrophysical Journal*. 1071.
[10.1086/500506](https://doi.org/10.1086/500506)

This Article is brought to you for free and open access by the Astronomy at ScholarWorks@UMass Amherst. It has been accepted for inclusion in Astronomy Department Faculty Publication Series by an authorized administrator of ScholarWorks@UMass Amherst. For more information, please contact scholarworks@library.umass.edu.

X-RAY ABSORPTION SPECTROSCOPY OF THE MULTI-PHASE INTERSTELLAR MEDIUM: OXYGEN AND NEON ABUNDANCES

YANGSEN YAO^{1,2} AND Q. DANIEL. WANG^{2,3}

Accepted for publication in the *Astrophysical Journal*

ABSTRACT

X-ray absorption spectroscopy provides a potentially powerful tool in determining the metal abundances in various phases of the interstellar medium (ISM). We present a case study of the sight line toward 4U 1820–303 (Galactic coordinates $l, b = 2^\circ.79, -7^\circ.91$ and distance = 7.6 kpc), based on *Chandra* Grating observations. The detection of O I, O II, O III, O VII, O VIII, and Ne IX $K\alpha$ absorption lines allows us to measure the atomic column densities of the neutral, warm ionized, and hot phases of the ISM through much of the Galactic disk. The hot phase of the ISM accounts for about 6% of the total oxygen column density $\sim 8 \times 10^{17} \text{ cm}^{-2}$ along the sight line, with the remainder about evenly divided between the neutral and warm ionized phases. By comparing these measurements with the 21 cm hydrogen emission and with the pulsar dispersion measure along the same sight line, we estimate the mean oxygen abundances in the neutral and total ionized phases as 0.3(0.2, 0.6) and 2.2(1.1, 3.5) in units of Anders & Grevesse (1989) solar value (90% confidence intervals). This significant oxygen abundance difference is apparently a result of molecule/dust grain destruction and recent metal enrichment in the warm ionized and hot phases. We also measure the column density of neon from its absorption edge and obtain the Ne/O ratio of the neutral plus warm ionized gas as 2.1(1.3, 3.5) solar. Accounting for the expected oxygen contained in molecules and dust grains would reduce the Ne/O ratio by a factor of ~ 1.5 . From a joint-analysis of the O VII, O VIII, and Ne IX lines, we obtain the Ne/O abundance ratio of the hot phase as 1.4(0.9, 2.1) solar, which is not sensitive to the exact temperature distribution assumed in the absorption line modeling. These comparable ISM Ne/O ratios for the hot and cooler gas are thus considerably less than the value (2.85 ± 0.07 ; 1σ) recently inferred from corona emission of solar-like stars (Drake & Testa 2005).

Subject headings: ISM: abundances — X-rays: ISM — X-rays: individual (4U 1820–303)

1. INTRODUCTION

The measurement of the ISM metal abundances plays a key role in our understanding of the universe. Although metals were all produced in stars, the ISM is the depository of stellar feedback (e.g., via supernovae). The metal abundances of the ISM thus give a unique measure of the integrated stellar feedback. The ISM is also a reservoir from which stars formed; the similarity or dissimilarity of the abundances in the ISM and stars provides important constraints on the physical processes involved in star formation and evolution (e.g., metal diffusion and settling). Of course, the abundances are also important in the study of various physical and chemical processes of the ISM itself (e.g., heating and cooling as well as dust grain formation). Furthermore, the interpretation of existing observational data often relies heavily on the assumption of the abundances in various phases of the ISM. Examples are the modeling of hot plasma spectra and the correction for ISM absorption to infer the intrinsic spectra of X-ray sources. Therefore, the measurement of the abundances represents a major task of astrophysics.

But a complete accounting of the metal abundances in the ISM has been a challenge. The ISM is a heterogeneous ensemble of various forms (atomic, molecular, and

solid dust grain) and various states (phases): cold ($\lesssim 100$ K), warm (~ 8000 K; including warm neutral and warm photo-ionized), and hot ($\sim 10^6$ K; collisionally ionized) (e.g., Ferrière 2001 and references therein). For easy of reference in the present work, we will not distinguish the cold and warm neutral phases and will call their combination as the “cold” phase. The “warm” phase will, instead, refer only to the above warm ionized phase; the total “ionized” phase therefore refers to a combination of warm and hot phases. Also these phases are used for the *atomic* gas form only, whereas molecule and solid dust grains are denoted as the “compound” form without any phase separation. The abundances of individual elements could be significantly different in these forms and phases, because of the varying level of depletion and molecule/grain destruction as well as recent chemical enrichment from stellar feedback. The traditional methods for abundance measurement in the optical and ultraviolet (UV) are sensitive mainly to the cold and warm phases. The reliability of such measurements strongly depends on how well the physical and ionization conditions are modeled (e.g., Savage & Sembach 1996 and references therein).

Stellar abundance measurements also suffer large uncertainties, especially for solar-like stars. Recently, solar abundances of light elements such as C, N, O and Ne have been revised downward by 25–45 per cent (Asplund, Grevesse, & Sauval 2005) from the values of Anders & Grevesse (1989; AG89 hereafter). The revised values reasonably agree with UV and X-ray measurements of the O abundance in the cold and warm ISM

¹ MIT Kavli Institute for Astrophysics and Space Research, 70 Vassar Street, Cambridge, MA 02139; yaoy@space.mit.edu

² Department of Astronomy, University of Massachusetts, Amherst, MA 01003; wqd@astro.umass.edu

³ Institute for Advanced Study, Einstein Drive, Princeton, NJ 08540

phases (e.g., Sofia & Meyer 2001; Takei et al. 2002; André et al. 2003; this work). However, this revision has broken the abundance accordance with helioseismological measurements and theoretical solar model predictions (e.g., Bahcall et al. 2005a). It is argued that the Ne abundance in the Sun is poorly determined and that if the Ne/O ratio is in fact substantially larger (by a factor of $\gtrsim 2.5$) the models can then be brought back into agreement with helioseismological measurements (e.g., Bahcall et al. 2005b). Based on the spectroscopy of the O VIII, Ne IX, and Ne X emission lines in the *Chandra* HETG-ACIS spectra of nearby solar-like stars, Drake & Testa (2005) estimate that the averaged Ne/O number ratio is 0.41 ± 0.01 (1σ), or 2.85 ± 0.07 of the AG89 value. However, two latest independent studies suggest no such high Ne/O ratio at the solar surface (Schmelz et al. 2005; Young 2005).

X-ray absorption spectroscopy can, in principle, be the ideal tool to measure the metal abundances of the ISM, in essentially all forms and phases. The X-ray bandpass contains almost all the K- and L-transitions of different charge states of the abundant elements from carbon to iron. X-ray spectroscopy, less affected by extinction, also probes larger column densities than is possible in the optical and UV, and is thus especially useful for measuring the general ISM through much of the Galactic disk. With the still limited spectral resolution and sensitivity of existing X-ray telescopes, however, only the most abundant elements (like oxygen and neon) can produce significant absorption features in the spectra of bright background sources such as AGNs and X-ray binaries. With the grating instruments aboard *Chandra* and *XMM-Newton*, several groups have indeed studied the abundances of X-ray-absorbing gas, based chiefly on measurements of absorption edges, which are contributed by the cold and warm phases in both atomic and compound forms (Paerels et al. 2001; Schulz et al. 2002; Takei et al. 2002; Juett & Chakrabarty 2003, 2005; Cunningham, McCray, & Snow 2004; Ueda et al. 2005). Most of these studies could only get relative metal abundances (e.g., Ne/O). But Takei et al. (2002) and Cunningham, McCray, & Snow (2004) were also able to estimate the absolute abundance (e.g., O/H) for the sight lines to Cyg X-2 and X Persei, by using emission line data (e.g, 21 cm) and UV absorption lines. Some success has been achieved even in distinguishing the contributions from the atomic and compound forms through calibrating the still uncertain wavelengths and cross-sections of the absorption edges (Takei et al. 2002).

More recently, Yao & Wang (2005; hereafter Paper I) and Wang et al. (2005; hereafter Paper II) have demonstrated the possibility of measuring the abundances of the hot ISM phase. By jointly fitting various highly-ionized species, significantly detected or not, one can simultaneously determine multiple parameters of the modeled absorbers such as the gas temperature, velocity dispersion, and element abundance ratio. Even with the limited counting statistics of the LMC X-3 observation, Wang et al. (2005) are able to obtain a meaningful lower limit to the Ne/O ratio, which is about the solar value of AG89.

We also note that the detection of O I, O II, and O III absorption lines allow for direct measurements of the cold and warm oxygen column densities. These lines have

large oscillator strengths relative to the expected velocity dispersions of the ISM phases; there is little flat part in the curve-of-growth (CoG) of such a line. Therefore, one can reliably measure the column densities in the typical square-root ranges of the CoG.

Here we capitalize on the high-quality detections of multiple absorption lines in the *Chandra* spectra of 4U 1820-303 (Futamoto et al. 2004; Paper I) to estimate the abundances in the multi-phase ISM of the Galaxy. Throughout this paper, we use the AG89 solar abundances as a convenient reference; the number ratios of O/H and Ne/O are 8.5×10^{-4} and 0.144; in comparison, the recently revised solar values are 4.6×10^{-4} and 0.151, respectively (Asplund, Grevesse, & Sauval 2005; further discussion in § 5). We also assume a collisional ionization equilibrium (CIE) in the hot intervening X-ray-absorbing gas; this should be quite a good approximation for the oxygen and neon in typical hot ISM conditions (Sutherland & Dopita 1993). The quoted parameter errors are all at 90% confidence levels unless otherwise specified.

2. 4U 1820-303 AND *Chandra* DATA CALIBRATION

4U 1820-303 is an exceptionally good target for the X-ray absorption spectroscopy of the ISM. First, this low mass X-ray binary (LMXB) is super compact, with an orbital period of only 685 s (Stella et al. 1987); the large ionization parameter in the immediate vicinity of the binary greatly reduces the chance for a significant local contribution to the observed absorption lines, consistent with their constancy, moderate ionization state, and insignificant width/shift (Futamoto et al. 2004; Paper I). Second, the binary resides in the globular cluster NGC 6624 ($l, b = 2^\circ.79, -7^\circ.91$, distance = 7.6 ± 0.4 kpc; Kuulkers et al. 2003) near the Galactic center (distance = 7.62 ± 0.32 kpc; Eisenhauer et al. 2005). Therefore, the pathlength of the sight line is well determined and samples the entire inner Galactic disk radially to a height of ~ 1 kpc off the Galactic plane. Third, the globular cluster also contains two radio pulsars, PSR 1820-30A and PSR 1820-30B, with essentially the same dispersion measure (DM) of $87 \text{ cm}^{-3} \text{ pc}$ or a total free electron column density of $N_e = 2.7 \times 10^{20} \text{ cm}^{-2}$ (Biggs et al. 1994), very useful for an absolute abundance measurement of ionized gas.

Chandra observed 4U 1820-303 three times: one observation used the low-energy transmission grating with the high resolution camera (LTEG-HRC; Brinkman et al. 2000) at the focal plane for 15 ks, and the other two used the high-energy transmission grating with the advanced CCD imaging spectrometer (HETG-ACIS; Canizares et al. 2005) for 9.7 and 10.9 ks, respectively. The LETG-HRC observation, particularly sensitive to O VII, has been reported by Futamoto et al. (2004), while the HETG-ACIS observations, sensitive to Ne IX, have been studied together with other targets by Juett, Schulz, & Chakrabarty (2004) and in Paper I. These studies have focused on either the global distribution of the intervening hot gas (Futamoto et al. 2004; Paper I) or on the oxygen absorption edge structure (Juett et al. 2004). Here we combine all these observations of 4U 1820-303, improving both the energy coverage and the counting statistics, to measure oxygen and neon abundances in the cold, warm, and hot phases.

We reprocess the three observations, using *CIAO* 3.2.1 and the calibration database CALDB 3.1.0⁴. We use *CIAO* thread *tgextract* to extract the source spectra. We rebin the MEG spectra to a bin size of 0.0125 Å so that they can be easily combined with the LETG spectrum. For each observation, we calculate the response matrices files (RMFs) and effective area files (ARFs) for the positive- and negative-grating arms by running scripts *mkgrmf* and *mkgarf*. For the HETG-ACIS observations, the effective area of the MEG is ~ 5 times larger than that of the high energy grating (HEG) in the wavelength band where our diagnostic absorption lines are located (e.g., longward of 13Å; Table 1). The effective area of the 1st orders is also at least one order of magnitude larger than that of the higher orders (≥ 2). Therefore, we only utilize the 1st order MEG spectra in this study. For the LETG-HRC observation, the detector has little intrinsic energy resolution, thus one needs to account for not only the local line spread but also the global spectral overlapping of different orders. We first calculate the RMFs and ARFs from the 1st to 6th grating orders [assuming the higher (> 6) order contribution to the spectrum in our interested wavelength range is negligible; see below] and then add these RMFs and ARFs pairs to form order-combined response files (RSPs; see Nicastro et al. 2005 and Paper II for more details). To improve the counting statistics, we further co-add the positive- and negative-grating MEG spectra and combine them with the LETG-HRC spectrum to form the final LETG+MEG spectrum. The corresponding RMFs and ARFs (RSPs) are averaged, channel by channel, with a globally modeled spectrum as the weighting function (similar to what is described below for the combined spectrum). We conduct various consistency checks for key results, based on the spectra from individual observations.

To account for the spectral order overlap, we model our combined spectrum over a broad range of 2-24.5 Å. As in previous studies (Nicastro et al. 2005 and Paper II), we fit the continuum with a combination of models: a blackbody (BB) and a broken power-law (BKNPL), plus ten broad ($\sigma > 1000 \text{ km s}^{-1}$) Gaussians (3 negative and 7 positive). These broad Gaussian features are used to compensate for both the deviation of the data from the simple BB+BKNPL combination and the calibration uncertainty in various gap/node regions. In addition, a foreground absorption with solar metal abundances is also applied. This continuum model gives a fit with $\chi^2/d.o.f=2448/1784$. The best-fit hydrogen column density is $N_H = 2.0 \times 10^{21} \text{ cm}^{-2}$, consistent with the values obtained from the optical extinction and H I 21 cm emission measurements (see § 4). This global fit is sufficiently accurate for our order overlap modeling. The HRC-LETG higher order contributions are relevant at wavelengths longward of 10 Å and are $\sim 7\%$ and 40% at 15 and 20 Å, respectively. Our subsequent spectroscopy is based primarily on local spectral data around individual absorption edge/lines considered. The spectral analysis uses the X-ray spectral analysis software package XSPEC (version 11.3.1).

3. ANALYSIS AND RESULTS

The detected O I, O II, O III, O VII, O VIII, and Ne IX $K\alpha$ absorption lines (see also Juett et al. 2004; Futamoto et al. 2004; Paper I) are clearly visible in our combined spectrum. We use six narrow negative Gaussian profiles to characterize these lines, which improves the spectral fit ($\chi^2/d.o.f=2042/1768$). Table 1 summarizes this Gaussian characterization of the absorption lines, including the velocity shifts (cz) relative to the adopted rest-frame wavelengths (λ) and the equivalent widths (EWs) as well as the significance of each line ($\Delta\chi^2$). We note that the O II $K\alpha$ line (Juett & Chakrabarty 2003) may be significantly contaminated by a weak oxygen compound line at $\sim 23.35 \text{ Å}$ (Takei et al. 2002). But the wavelength and oscillator strength of the line (or complex) are very uncertain, and depend on the exact composition of the compound. All the observed lines are unresolved; the instrument resolution gives an upper limit $\sim 500 \text{ km s}^{-1}$ to the velocity dispersion ($\sqrt{2}$ times the Gaussian width) of the O VII $K\alpha$ line. We also obtain an upper limit to the EW of the O VII $K\beta$ line by fixing its centroid and linking its velocity dispersion with that of O VII $K\alpha$ (Table 1). This Gaussian characterization of the lines is consistent with previous studies (Futamoto et al. 2004; Juett et al. 2004; Paper I), although our present results have smaller uncertainties because of the improved counting statistics in the LETG+MEG spectrum. Since all the lines, except for O VII $K\beta$, are saturated, the EWs (presented here only for ease of comparison with similar analyses) could be strongly biased due to the inaccuracy of the Gaussian characterization (Paper I) and should thus be interpreted with caution.

Our analyses and results, presented in the following sections, are based on the recently constructed absorption line model *absline*, as detailed in Paper I. This model adopts the accurate *Voigt* function as the line profile, accounting for line saturation automatically and allowing for a joint-fit to multiple absorption lines. The basic model parameters are the line centroid E_l , velocity dispersion b_v , and reference ionic column density N_X (e.g., $X=O \text{ VII}$ or H). In a fit to multiple lines, other parameters can be included, such as the temperature T and metal abundance(s) Z_X . Such a fit can be much more powerful than a simple CoG analysis: e.g., parameters such as the velocity dispersion can be measured from relative line saturations, and statistical uncertainties in multiple parameters can be easily determined. Paper II includes a detailed comparison of the *absline* model with the CoG analysis, which is more illustrative but less powerful in the present context.

3.1. Cold and Warm Phases

We fit the O I, O II, and O III $K\alpha$ lines, individually, with the *absline* model [Fig. 1 (a)]. We assume a velocity dispersion $b_v = 62 \text{ km s}^{-1}$, inferred from the Al III absorption line in the high-resolution far-UV spectrum of HD 163522, a star in an adjacent direction of (l, b)=(350°, -9°) and at a distance of $\sim 9 \text{ kpc}$ (Savage, Sembach, & Massa 1990). The fitted column densities are $\log[N_{\text{OI}}(\text{cm}^{-2})] = 17.6(17.3, 17.9)$, $\log[N_{\text{OII}}(\text{cm}^{-2})] = 17.4(16.9, 17.6)$, and $\log[N_{\text{OIII}}(\text{cm}^{-2})] = 17.0(16.5, 17.5)$. These values are not very sensitive to the exact choice of the assumed b_v value, because these X-ray absorption lines are in the saturated square-root range of the CoG (§1); a factor of

⁴ <http://xc.harvard.edu/ciao/download>

TABLE 1
LINE PARAMETERS AND GAUSSIAN FIT RESULTS

line	λ (\AA)	f_{ij}	$\Delta\chi^2$	cz (km s^{-1})	EW (m\AA)
O I $K\alpha$	23.508	0.431	205	4(-92, 124)	83(66, 141)
O II $K\alpha$	23.352	0.424	36	1(-287, 106)	86(52, 173)
O III $K\alpha$	23.106	0.141	28	251(-47, 550)	74(41, 109)
O VII $K\alpha$	21.602	0.696	49	204(89, 328)	40(30, 53)
O VII $K\beta$	18.627	0.146	2	fixed	< 10
O VIII $K\alpha$	18.967	0.277	34	-48(-215, 119)	19(13, 25)
Ne IX $K\alpha$	13.448	0.657	52	-35(-213, 68)	9(7, 11)

NOTE. — The rest-frame wavelength (λ) values of the O I, O II, and O III $K\alpha$ absorption lines are from averages over multiple detections; absolute theoretical values are still quite uncertain (see Juett et al. 2004; Paper II). The transition oscillator strength f_{ij} values of these lines are from García et al. (2005). The λ and f_{ij} values of the other lines are as in Paper I. $\Delta\chi^2$ is the χ^2 reduction when the corresponding line is included in the spectral fit.

two variation in b_v , for example, would cause a change $\lesssim 20\%$ in these column densities, which is smaller than the statistical uncertainties. For O I, in particular, we find that the column density changes by $\lesssim 10\%$ when b_v changes from 62 to 0 km s^{-1} . Systematically, however, N_{OII} might be over-estimated because the potential confusion with compound oxygen absorption (e.g., Takei et al. 2002; further discussion in §4).

These column density estimates, based on absorption lines, may be compared with the absorption edge results of Juett et al. (2004) from the same source. They measured the column density of oxygen only in the atomic form, although the atomic edges are embedded within similar structures produced by oxygen in the compound form. The compound edge structures are at lower energies and are less well defined than the atomic ones because of such uncertain factors as grain and molecule composition and confusion with various absorption lines (Juett et al. 2004; Takei et al. 2002). In addition to atomic edges, Juett et al. (2004) also focused on the identification and calibration of the $K\alpha$ lines from O I, O II, and O III. Their analysis was based on HETG observations of seven X-ray binaries, including 4U 1820–303. Toward this source, they first obtained an oxygen column density of $1.31(1.17, 1.51) \times 10^{18} \text{ cm}^{-2}$ from the edge measurement and then predicted an EW of the O I $K\alpha$ absorption line. This EW is, however, significantly higher than the observed value. Similar offsets are also apparent for most of the other sight lines. They tentatively attributed this difference to their use of the Gaussian line function, instead of the more accurate Voigt profile. While the latter profile is used in our analysis, the offset for 4U 1820–303 remains; i.e., our measured O I column density $4.0(2.0, 7.9) \times 10^{17} \text{ cm}^{-2}$ is substantially smaller than the oxygen column density from the edge measurement. In fact, an offset is expected because the oxygen absorption edge includes contributions not only from O I, as is traced by its $K\alpha$ line, but also from the oxygen in the compound form and from O II and O III in the warm phase of the ISM. The sum of our measured column densities of O I, O II, and O III gives $N(\text{O I}+\text{O II}+\text{O III})=0.75(0.48, 1.22) \times 10^{18} \text{ cm}^{-2}$, which is in a better agreement with the edge measurement.

The remaining small discrepancy is likely caused by a slight over-estimate of the atomic oxygen column density from the edge measurement, presumably because of neglecting the compound contribution, as acknowledged by Juett et al. (2004). Furthermore, their edge model as plotted seems to overpredict the absorption at the edge ($\lesssim 23 \text{ \AA}$; see their Fig. 4).

We can also measure the column density of neon based on its absorption edge. Because neon is a noble element and is not easily in a compound form, the absorption edge structure is much simpler than that of oxygen. But, in the HETG observations, the neon edge of the MEG negative grating arm data unfortunately lands in a CCD gap, and there are also some complicated instrumental features around the edge wavelength of the positive arm data. We thus use only the LETG spectrum for the neon edge measurement. We fit the spectrum in the wavelength range of 2–24.5 \AA with the XSPEC *varabs* model, assuming the solar abundances, except for the neon, which is modeled separately with the XSPEC *edge* model (Fig. 2). We obtain the neon edge wavelength $\lambda_E = 14.28(14.23, 14.35) \text{ \AA}$ and optical depth $\tau_E = 8.6(7.0, 10.2) \times 10^{-2}$. Adopting the neon absorption cross section of $3.67 \times 10^{-19} \text{ cm}^{-2}$ from Bałucińska-Church & McCammon (1992), we derive the neon column density as $N_{\text{Ne}} = 2.3(1.9, 2.7) \times 10^{17} \text{ cm}^{-2}$.

By combining these measurements of the oxygen and neon column densities, we further estimate the Ne/O ratio in the cold plus warm gas as $(\text{Ne/O})_{\text{cw}} = N_{\text{Ne}}/N(\text{O I}+\text{O II}+\text{O III}) = 0.3(0.2, 0.5)$, or $2.1(1.3, 3.5)$ solar.

3.2. Hot Phase

We first consider the X-ray absorption by hot gas of a single temperature and a single velocity dispersion (neglecting the small ion mass differences between oxygen and neon). Adopting O VII as the reference ion, Table 2 illustrates, step by step, the dependence of parameter constraints on the inclusion of individual absorption lines. The logic in the parameter constraints in each step is described in the following:

1. Fitting the O VII $K\alpha$ absorption line alone provides an upper limit to b_v (determined by the instrument

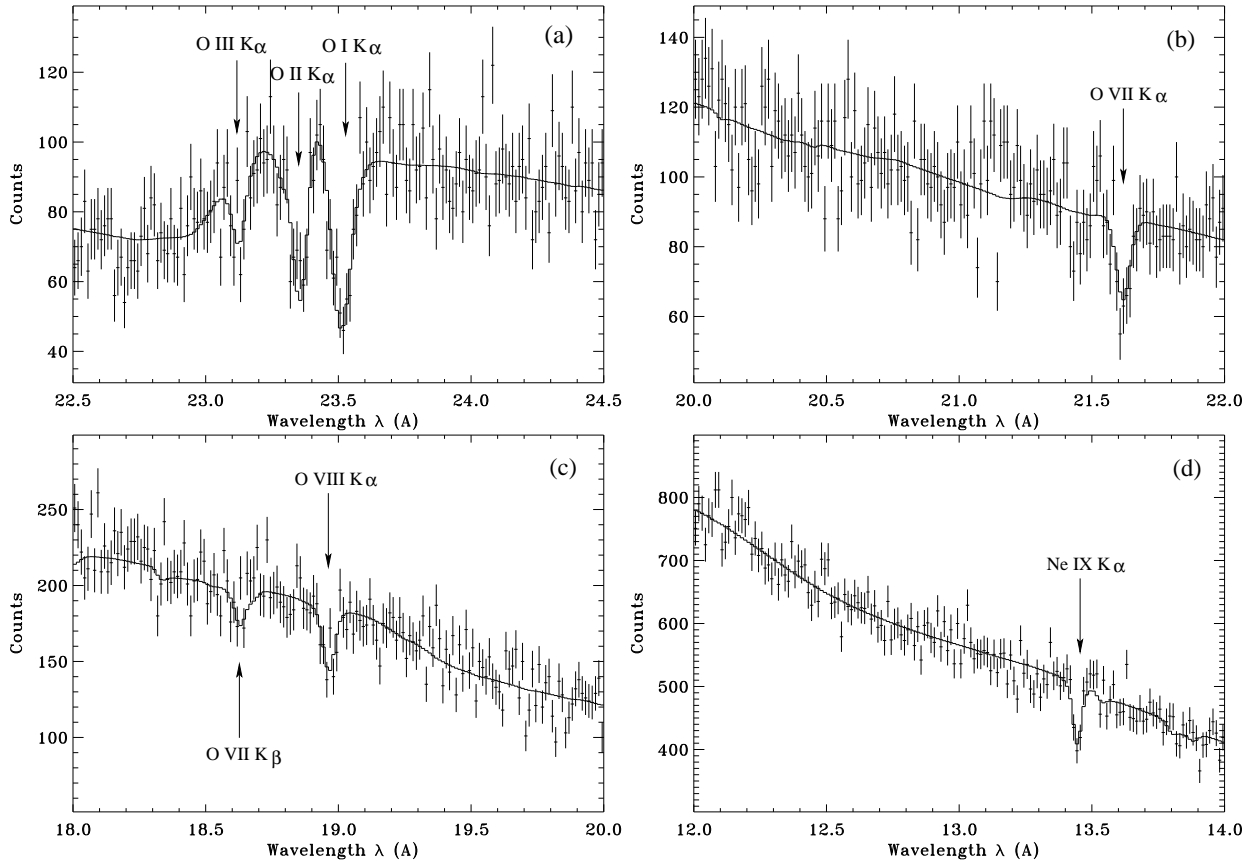


FIG. 1.— The oxygen and neon absorption lines in the LETG+MEG spectrum (with a bin size of 0.0125 \AA), together with the best-fit *absline* model plus the continuum. The ARF and RMF have been applied to the model. The local $\chi^2/d.o.f.$ are 156/130 (a), 146/154 (b), 203/153 (c), and 177/153 (d). The wavelength is marked for the 1st order, although the spectra are also contributed by higher orders. The O VII K β (c), although not significantly detected, is included in the fit. See text for detail.

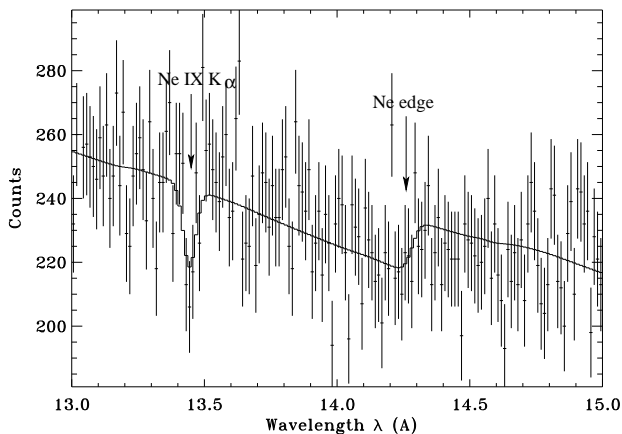


FIG. 2.— The Ne edge and the Ne IX K α absorption line in the HRC-LETG spectrum, fitted with XSPEC *edge* plus *absline* models ($\chi^2/d.o.f. = 150/144$). The bin size is 0.0125 \AA ; the ARF and RMF have been applied to the model. The rest is the same as in Fig. 1.

resolution) and a corresponding lower bound to N_{OVII} (whereas its upper limit corresponds to $b_v \simeq 0 \text{ km s}^{-1}$).

2. Jointly fitting the O VII K α and K β lines gives a lower limit to b_v and therefore an improved upper limit to N_{OVII} . Because both lines trace the same ion, an extremely small b_v would make the O VII K α line too sat-

urated to be consistent with the observed O VII K β /K α constraint.

3. The inclusion of the O VIII line gives a measurement of T (assuming a uniform isothermal CIE plasma origin for the lines).

4. Finally, the Ne IX line, together with the measurement of T in Step 3, constrains the neon column density. The comparison of the neon and oxygen column densities then leads to the estimate of the Ne/O ratio.

The line centroid shifts obtained from the final joint-fit [Fig. 1 (b)-(d)] are nearly the same as those obtained from the Gaussian model fits (Table 1). The parameters (T , b_v , and N_{OVII}), though more tightly constrained here, are still consistent with those found in the previous studies within the quoted error ranges (Futamoto et al. 2004; Paper I). But the measurement of the Ne/O ratio here is completely new. Fig. 3 shows the confidence contours of the Ne/O ratio vs. T .

One may expect variation in physical and chemical properties of the hot gas along the sight line to 4U 1820–303. The so-called Local Bubble around the Sun, for example, is believed to contain hot gas with $T \sim 10^6 \text{ K}$ (e.g., Kuntz & Snowden 2000), lower than the average value along the sight line (Table 2). Because the Sun is not supposed to be at a “privileged” spot in the Galaxy, it is natural to assume that much of the Galactic disk is occupied by such bubbles, and that somewhat hotter versions of which may be responsible for the ubiq-

TABLE 2
STEP-BY-STEP *absline* FITS TO HOT GAS ABSORPTION LINES

Step	Included line(s)	b_v (km s ⁻¹)	$\log N_{\text{OVII}}$ (cm ⁻²)	$\log T$ (K)	Ne/O
1	O VII K α	< 446	17.2(16.3, 18.7)
2	O VII K α , K β	298(169, 505)	16.3(16.1, 16.5)
3	O VII K α , K β , O VIII K α	325(197, 490)	16.3(16.1, 16.5)	6.34(6.29, 6.41)	...
4	O VII K α , K β , O VIII K α , Ne IX K α	255(165, 369)	16.3(16.1, 16.5) ^a	6.34(6.29, 6.41)	1.4(0.9, 2.1) ^b

NOTE. — ^a The equivalent hydrogen, O VIII, and Ne IX column densities are $\log[N_H(\text{cm}^{-2})]=20.1(19.9, 20.2)$, $\log[N_{\text{OVIII}}(\text{cm}^{-2})]=16.4(16.2, 16.6)$, and $\log[N_{\text{NeIX}}(\text{cm}^{-2})]=16.0(15.9, 16.1)$. ^b The Ne/O ratio is in units of the AG89 solar number ratio.

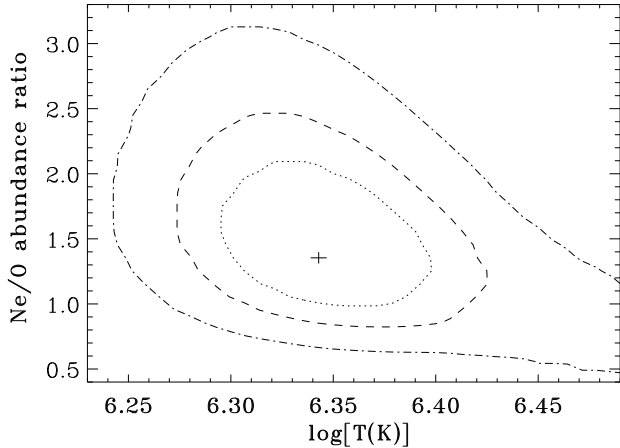


FIG. 3.— The 60%, 90%, and 99% confidence contours of the Ne/O ratio and gas temperature, as obtained in the final joint-fit of the hot gas X-ray absorption lines with the *absline* model (Step 4 in Table 2).

uitous 3/4 keV background emission (Snowden et al. 1997). X-ray absorption line spectroscopy of multiple sight lines has also shown evidence for the presence of a thick Galactic disk with a scale height of 1-2 kpc (Yao & Wang 2005). Furthermore, the Galactic bulge is apparently enhanced in X-ray emission (Snowden et al. 1997), although whether it arises mostly from unresolved point-like sources or truly diffuse hot gas is yet to be determined. A preliminary comparison of the 4U 1820–303 sight line with those toward LMC X–3 ($l, b = 273^\circ.58, -32^\circ.08, D = 50$ kpc; Paper II) and 4U 1957+11 (V1408 Aql; $l, b = 51^\circ.31, -9^\circ.33, D = 5.5$ kpc; Yao et al. in preparation) shows that the averaged temperature of the hot gas along the sight line through the bulge appears hotter by a factor of ~ 1.5 .

Though without a detailed knowledge about the hot gas variation, we can still check its effect on our absorption line measurements. Because the size of a bubble similar to the local one is small (dimension $\sim 10^2$ pc), its individual contribution (e.g., $N_{\text{OVII}} \lesssim 3 \times 10^{15}$ cm⁻²; Fang, Sembach, & Canizares (2003)) is negligible, compared to the observed total absorption toward 4U 1820–303 (Table 2). Therefore, we can characterize the variation within a bubble and/or from one bubble to another along a sight line by using a dispersion around a mean parameter (e.g., T). This dispersion may also include any Galaxy-wide variation. Here we test how the Ne/O ratio may be influenced if the isothermal assumption is

relaxed by adopting a simple extension to a log-Gaussian temperature distribution:

$$dN(T) \propto e^{-\frac{(\log T - \log T_0)^2}{2(\sigma_{\log T})^2}} d\log(T), \quad (1)$$

where T_0 is equivalent to T in the isothermal case and is in units of K, while $\sigma_{\log T}$ is the dispersion of $\log T$. After revising our *absline* model to incorporate this distribution, we repeat the final joint-fit again. This fit gives a 90% upper limit of 0.84 to the new parameter $\sigma_{\log T}$. As shown in the upper panel of Fig. 4, there is a strong correlation between $\log T_0$ and $\sigma_{\log T}$; i.e., the fit prefers a higher centroid temperature T_0 when the dispersion is broader. This correlation results from the observed strong O VIII absorption line, which arises only in a narrow and relatively high temperature range [$\log T(\text{K}) \sim 6.35 - 6.50$], compared to O VII, which dominates over a much broader and lower temperature range (see Fig. 1 in Paper I). The lower panel of Fig. 4 shows that the inferred Ne/O ratio is insensitive to $\sigma_{\log T}$. A similar conclusion is also reached in our test with a power law temperature distribution.

4. OXYGEN ABUNDANCES

In addition to the preceding X-ray oxygen column density and Ne/O ratio results, we can also estimate the absolute oxygen abundances (O/H). Such estimates, however, cannot be made for all individual phases separately, due to the lack of required measurements. For example, we cannot separately estimate the Ne/O ratios in the cold and warm phases, because the Ne edge data do not allow for individual measurements of the corresponding neon column densities. Table 3 summarizes the results for various ISM phases and/or their combinations. To estimate an absolute oxygen abundance, we need to know the hydrogen column density in the same phase and in the same form. Because 4U 1820–303 is located above the H I disk of the Galaxy, we can use the hydrogen column density from the 21 cm emission line survey in the source field, $N(\text{H I}) = 1.5 \times 10^{21}$ cm⁻² (Dickey & Lockman 1990)⁵, which may be compared to a total cold hydrogen column density $N(\text{H I}) + 2N(\text{H}_2) \simeq 1.9 \times 10^{21}$ cm⁻² inferred from the optical extinction of the global cluster $E(B - V) \simeq 0.32$ (Bohlin, Savage, & Drake 1978;

⁵ We use this easily accessible data base, instead of the newer, probably more reliable Leiden-Argentine-Bonn HI survey (Kalberla et al. 2005). The difference ($\sim 15\%$) between the two survey values is much less than the statistical uncertainties in the derived parameters.

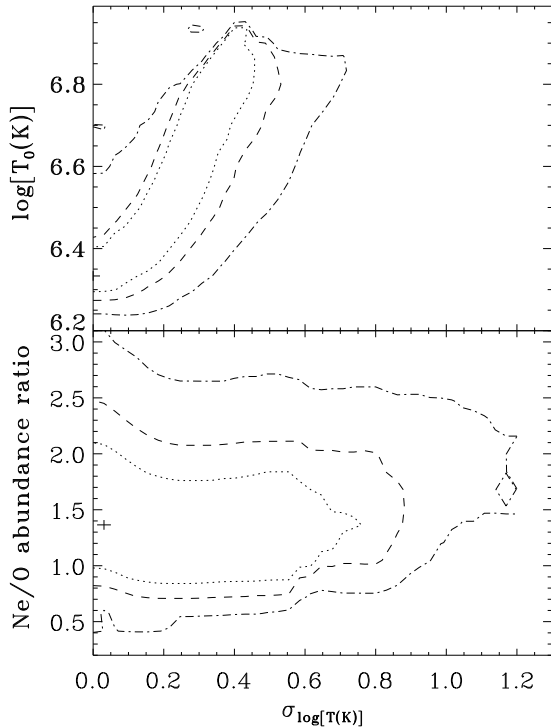


FIG. 4.— The 68%, 90%, and 99% confidence contours for the log-Gaussian temperature distribution.

TABLE 3
SUMMARY OF RESULTS

Parameter	Gas Phase		
	cold	warm	hot
	column density		
O	17.6(17.3, 17.9)	17.5(17.2, 17.8) ^a	16.7(16.5, 16.8) ^b
H	21.2 ^e	17.9(17.7, 18.1) ^c	17.6(17.3, 17.8) ^d
Ne	17.4(17.3, 17.5) ^c	20.4 ^{d,f}	16.0(15.9, 16.1)
	Abundance ^g		
O/H	0.3(0.2, 0.6)	2.0(0.8, 3.6)	$\gtrsim 0.94$
Ne/O	2.1(1.3, 3.5) ^c	2.2(1.1, 3.5) ^d	1.4(0.9, 2.1)

NOTE. — The column densities are all on a logarithmic scale. The values for the cold and warm oxygen phases are obtained from the fits to individual lines (O I K α , O II K α , and O III K α), whereas the values for the hot phase are obtained from a joint-fit to multiple lines (O VII K α , K β , O VIII K α , and Ne IX K α). ^a N(O II+O III), which may be over-estimated because of the contamination from a potential compound oxygen line that is not accounted for. ^b N(OVII+OVIII). ^c Cold plus warm gas. ^d Warm plus hot (ionized) gas. ^e The 21 cm emission data are used. ^f The pulsar dispersion measure is used. ^g All abundances and ratios are listed in units of the AG89 solar values (i.e., O/H = 8.5×10^{-4} and Ne/O = 0.144).

Kuulkers et al. 2003). We estimate oxygen abundance in the cold phase as $(\text{O}/\text{H})_n = N(\text{O I})/N(\text{H I}) = 2.6(1.3, 5.3) \times 10^{-4}$, or $0.3(0.2, 0.6)$ AG89 solar.

For ionized gas, we can use the free electron column density N_e from the pulsar DM (§2). The oxygen column densities in the warm and hot phases are $N(\text{O II}+\text{O III})$ and $N(\text{OVII}+\text{OVIII})$, neglecting O IV - O VI and O IX, which are only important in thermally very unstable “intermediate” temperatures ($T \lesssim 10^{5.5}$ K) and in probably rare low-density regions with temperatures $\gtrsim 10^{6.5}$

K. We can then define the oxygen abundances in the two phases as $(\text{O}/\text{H})_w = N(\text{O II}+\text{O III})/\eta(1-\xi)N_e$ and $(\text{O}/\text{H})_h = N(\text{O VII}+\text{O VIII})/\xi\eta N_e$, where ξ is the hot phase fraction of the electrons and $\eta = 0.84$ accounts for the contribution from helium. Letting $(\text{O}/\text{H})_h = \alpha (\text{O}/\text{H})_w$, we have $\xi = 1/(1 + \alpha r_N)$, where $r_N = N(\text{O II}+\text{O III})/N(\text{O VII}+\text{O VIII}) \sim 8$. We expect that dust grain destruction and chemical enrichment occurs primarily in the hot phase; i.e., the metal abundance in the hot phase should be comparable to, or higher than, that in the warm phase. Therefore, $\alpha \gtrsim 1$; specifically, $(\text{O}/\text{H})_w = 1.8(0.8, 3.1) \times 10^{-3}$ for $\alpha = 1$ and $1.6(0.7, 2.8) \times 10^{-3}$ for $\alpha = \infty$. We thus adopt $1.7(0.7, 3.1) \times 10^{-3}$ [or $2.0(0.8, 3.6)$ solar] to account for this small α -dependent uncertainty. Systematically, however, this oxygen abundance could be an overestimate, because of the potential contamination to the O II line by the uncertain compound oxygen line as mentioned in § 3. For instance, if the compound oxygen column density is $\sim 0.5N_{\text{OI}}$, as suggested by Takei et al. (2002), then $(\text{O}/\text{H})_w \sim 9.2 \times 10^{-4}$ and 6.7×10^{-4} for $\alpha = 1$ and ∞ , respectively. On the other hand, $(\text{O}/\text{H})_h \propto \alpha$ cannot be determined without knowing α . Nevertheless, we may estimate the mean oxygen abundance in total ionized gas: $[N(\text{OII} + \text{OIII}) + N(\text{OVII} + \text{OVIII})]/\eta N_e = 2.2(1.1, 3.5)$ solar, or ~ 1.1 solar if the potential contamination from the compound oxygen is accounted for.

5. COMPARISONS WITH OTHER ABUNDANCE MEASUREMENTS

Not all X-ray binaries are suitable background sources for ISM measurements. High mass X-ray binaries (HMXBs) suffer potentially serious stellar contamination to absorption features. The observed X-ray-absorbing column density of the HMXB Cyg X-1, for example, shows an orbital dependence (Ebisawa et al. 1996; Schulz et al. 2002). Even LMXBs could be problematic. There are previous Ne/O measurements based on absorption edge data of several LMXBs (Paerels et al. 2001; Juett & Chakrabarty 2003, 2005). Higher Ne/O ratios (up to a factor of several times the solar value) are sometimes reported and are suggested to be local to the binary systems, which typically show burst behaviors and are proposed to have neon-rich white dwarf companions. The discovery of the Ne/O ratio variation with time in two of such sources supports this scenario (Juett & Chakrabarty 2005; Sidoli et al. 2005).

Relatively secure X-ray estimates of the ISM oxygen and neon abundances in previous studies are available only for the sight line to Cyg X-2 (Takei et al. 2002). With its Galactic position ($l, b = 87^\circ.33, -11^\circ.32$ and distance = 7.2 kpc), the sight line samples gas primarily at the solar radius of the Galaxy, providing an interesting comparison with the inner Galactic disk sight line to 4U 1820-303. Similar to 4U 1820-303, Cyg X-2 is located at a large off-Galactic plane distance, allowing reasonable estimates of the hydrogen column densities along the sight line from 21 cm, H α , and CO emission lines. Takei et al. (2002) estimated that the oxygen abundance is $\sim 0.47 \pm 0.16$ solar in the atomic gas and a factor of ~ 1.5 higher in the atomic plus compound ISM. Their estimates are based on the absorption edges, which are dominated by the cold and warm phases. Although our oxy-

gen measurements are based on the absorption lines, we can derive an average oxygen abundance for the cold plus warm gas along the sight line to 4U 1820–303 (Table 3), $N(\text{O I}+\text{O II}+\text{O III})/[N(\text{HI})+(1-\xi)\eta N_e]=0.52(0.33, 0.85)$ solar. This value is consistent with the oxygen abundance estimate along the sight line to Cyg X–2.

Our neon abundance measurement of the cold plus warm gas along the sight line to 4U 1820–303 is based on the absorption edge, as it is to Cyg X–2 (Takei et al. 2002). The neon abundance 0.75(0.55, 0.95) toward this latter source is considerably lower than 1.2(1.0, 1.4) inferred here for the sight line to 4U 1820–303, which indicates a moderately metal enhancement in the inner region compared to the outer region of the Galaxy. The Ne/O ratios along these two sight lines are compatible [2.1(1.3, 3.5) vs. 1.6(0.9, 2.3)]. For 4U 1820–303, we also have the hot Ne/O ratio 1.4(0.9, 2.1), comparable to the value in the cold plus warm gas, particularly if the expected oxygen compound contribution is included. The hot Ne/O ratio, if typical in the Galaxy, can be used in a joint analysis of oxygen and neon X-ray absorption lines observed in other sight lines.

Now let us compare our inferred ISM Ne/O ratios with those stellar measurements. At first glance, our Ne/O ratio [$\sim 2.1(1.3, 3.5)$] obtained for the cold plus warm gas is consistent with the high Ne/O ratio as suggested by Drake & Testa (2005). But, including as well the expected oxygen compound contribution would then lead to a reduced Ne/O ratio (by a factor of ~ 1.5 ; Takei et al. 2002) that would be significantly lower than the stellar ratio. Similarly, our inferred hot gas Ne/O ratio (Table 3) is significantly lower (by $\sim 3\sigma$) than the stellar value. It is difficult to reconcile this Ne/O ratio difference and the total oxygen abundance similarity between the stellar and ISM measurements. There is no obvious way to hide neon in the ISM! We suspect that the Ne/O ratio estimate from stellar emission lines, which is generally sensitive to modeling assumptions, may not represent the true underlying composition of the stars. The inconsistency of the stellar measurements by Drake & Testa (2005) with the recent solar studies (Schmelz et al. 2005; Young 2005) illustrates such an uncertainty.

6. SUMMARY

We have used the *Chandra* HETG and LETG observations of the LMXB 4U 1820–303 as a test case to explore the potential for metal abundance measurement in different atomic phases of the ISM. We have concentrated on the measurements of atomic oxygen and neon, as summarized in Table 3, and on comparison with previous X-ray studies. Our main results and conclusions are as follows:

1. We have separately measured the column densities of O I, O II, and O III from their heavily saturated $K\alpha$ lines. These measurements are only weakly dependent on the exact velocity dispersion assumed. A comparison of

the O I column density and the 21 cm hydrogen emission in the field gives a cold (neutral) oxygen abundance of 0.3(0.2, 0.6) solar (AG89). The ratio of our measured O II plus O III column density to the pulsar DM along the same sight line further gives an estimate of the warm oxygen abundance as 2.0(0.8, 3.6) solar.

2. We have constrained the neon column density from its absorption edge, giving an abundance of 1.2(1.0, 1.5) solar and a Ne/O ratio of 2.1(1.3, 3.5) solar for the cold plus warm gas. The Ne/O ratio with the inclusion of the compound ISM is likely to be a factor of ~ 1.5 lower (Takei et al. 2002).

3. We have also measured the oxygen column density and Ne/O ratio in the hot ISM, based on a joint-analysis of the detected O VII $K\alpha$, O VIII $K\alpha$, and Ne IX $K\alpha$ absorption lines, together with the non-detection of the O VII $K\beta$ line. Assuming that O VII $K\alpha$ and O VIII $K\alpha$ trace all hot gas (i.e., $T \sim 10^{5.5-6.5}$ K), we estimate that the hot phase accounts for about 6% of the total oxygen column density along the sight line and obtain a Ne/O ratio of 1.4(0.9, 2.1) solar, which is insensitive to the exact temperature distribution assumed.

4. Our abundance estimates for the atomic phases, together with complementary X-ray spectroscopic studies of the total abundances, may have strong implications for understanding various chemical enrichment and depletion processes both in the ISM and during star formation. There is evidence for an enhanced enrichment in the hot gas, especially in comparison with the cold phase. The Ne/O ratios obtained in the ISM are significantly smaller than the value indicated in the recent emission line measurement of solar-like stars (Drake & Testa 2005).

The existing X-ray measurements of the ISM abundances (including the present work) are still preliminary, subject to various systematic uncertainties, both theoretical and observational, which are yet difficult to fully quantify. Nevertheless, the outcome of this study demonstrates the unique potential for a comprehensive characterization of the metal abundances in various ISM forms and phases.

We thank Daniel Dewey, Edward Jenkins, and Blair Savage for reading an early draft of the paper and for providing valuable comments and suggestions. We also thank the referee for valuable suggestions which helped to improve the presentation of the paper. We are grateful to Todd Tripp, Paola Testa, and Norbert Schulz for useful discussions. Support for this work was partially provided by NASA through the Smithsonian Astrophysical Observatory (SAO) contract SV3-73016 to the MIT for support of the *Chandra* X-Ray Center, which is operated by the SAO for and on behalf of NASA under contract NAS 8-03060. Support from a *Chandra* archival research grant is acknowledged.

REFERENCES

- Anders, E., & Grevesse, N. 1989, *Geochim. Cosmochim. Acta*, 53, 197
- André, M. K., Oliveira, C. M., Howk, J. C., Ferlet, R., Désert, J.-M., Hébrard, G., Lacour, S., Lecavelier des Étang, A., Vidal-Madjar, A., & Moos, H. W. 2003, *ApJ*, 591, 1000
- Asplund, M., Grevesse, N., & Sauval, J. 2005, *ASPC*, 336, 25
- Bahcall, J. N., Basu, S., Pinsonneault, M., & Serenelli, A. M. 2005a, *ApJ*, 618, 1049
- Bahcall, J. N., Basu, S., & Serenelli, A. M. 2005b, *ApJ*, 631, 1281
- Bałucińska-Church, M., & McCammon, D. 1992, *ApJ*, 400, 699
- Biggs, J. D., Baines, M., Lyne, A. G., Goss, W. M., & Fruchter, A. S. 1994, *MNRAS*, 267, 125
- Bohlin, R. C., Savage, B. D., & Drake, J. F. 1978, *ApJ*, 224, 132

- Brinkman, A. C., Gunning, C. J. T., Kaastra, J. S., van der Meer, R. L. J., Mewe, R., Paerels, F., Raassen, A. J. J., van Rooijen, J. J., Bräuning, H., Burkert, W., et al. 2000, *ApJ*, 530, L111
- Canizares, C. R., Davis, J. E., Dewey, D., Flanagan, K. A., Galton, E. B., Huenemoerder, D. P., Ishibashi, K., Markert, T. H., et al. 2005, *PASP*, 117, 1144
- Cunningham, N. J., McCray, R., & Snow, T. P. 2004, *ApJ*, 611, 353
- Dickey, J. M., & Lockman, F. J. 1990, *ARA&A*, 28, 215
- Drake, J. J., & Testa, P. 2005, *Nature*, 436, 525
- Ebisawa, K., Ueda, Y., Inoue, H., Tanaka, Y., & White, N. E. 1996, *ApJ*, 467, 419
- Eisenhauer, F., Genzel, R., Alexander, T., Abuter, R., Paumard, T., Ott, T., Gilbert, A., Gillessen, S., et al. 2005, *ApJ*, 628, 246
- Fang, T., Sembach, K. R., & Canizares, C. R. 2003, *ApJ*, 586, L49
- Ferrière, K. 2001, *Rev. Mod. Phys.*, 73, 1031
- Futamoto, K., Mitsuda, K., Takei, Y., Fujimoto, R., & Yamasaki, N. Y. 2004, *ApJ*, 605, 793
- García, J., Mendoza, C., Bautista, M. A., Gorczyca, T. W., Kallman, T. R., & Palmeri, P. 2005, *ApJS*, 158, 68
- Juett, A., & Chakrabarty, D. 2003, *ApJ*, 599, 498
- Juett, A., Schulz, N., & Chakrabarty, D. 2004, *ApJ*, 612, 308
- Juett, A., & Chakrabarty, D. 2005, *ApJ*, 627, 926
- Kalberla, P. M. W., Burton, W. B., Hartmann, Dap, Arnal, E. M., Bajaja, E., Morras, R., Pöppel, W. G. L. 2005, *A&A* 440, 775
- Kunt, K. D., & Snowden, S. L. 2000, *ApJ*, 543, 195
- Kuulkers, E., den Hartog, P. R., in't Zand, J. J. M., Verbunt, F. W. M., Harris, W. E., & Cocchi, M. 2003, *A&A*, 399, 663
- Nicastro, F., Mathur, S., Elvis, M., Drake, J., Fiore, F., Fang, T., Fruscione, A., Krongold, Y., Marshall, H., & Williams, R. 2005, *ApJ*, 629, 700
- Paerels, F., Brinkman, A. C., van der Meer, R. L. J., Kaastra, J. S., Kuulkers, E., Boggende, A. J. F. den, Predehl, P., Drake, J.; Kahn, S. M., Savin, D. W., & McLaughlin, B. M. 2001, *ApJ*, 546, 338
- Savage, B., Sembach, K. R., & Massa, D. 1990, *ApJ*, 355, 114
- Savage, B., & Sembach, K. R. 1996, *ARA&A*, 34, 279
- Schmelz, J. T., Nasraoui, K., Roames, J. K., Lippner, L. A., & Garst, J. W. 2005, *astro-ph/0510230*
- Schulz, N. S., Cui, W., Canizares, C. R., Marshall, H. L., Lee, J. C., Miller, J. M., & Lewin, W. H. G. 2002, *ApJ*, 565, 1141
- Sidoli, L., La Palombara, N., Oosterbroek, T., & Parmar, A. N. 2005, *A&A*, in press (*astro-ph/0507242*)
- Snowden, S. L., Egger, R., Freyberg, M. J., McCammon, D., Plucinsky, P. P., Sanders, W. T., Schmitt, J. H. M. M., Truemper, J., & Voges, W. 1997, *ApJ*, 485, 125
- Sofia, U. J., & Meyer, D. M. 2001, *ApJ*, 554, L221
- Stella, L., Priedhorsky, W., & White, N. E. 1987, *ApJ*, 312, L17
- Sutherland, R. S., & Dopita, M. A. 1993, *ApJS*, 88, 253
- Takei, Y., Fujimoto, R., Mitsuda, K., & Onaka, T. 2002, *ApJ*, 581, 307
- Ueda, Y., Mitsuda, K., Murakami, H., & Matsushita, K. 2005, *ApJ*, 620, 274
- Wang, Q. D., Yao, Y., Tripp, T. M., Fang, T.-T., Cui, W., Nicastro, F., Mathur, S., Williams, R., Song, L., & Croft, R. 2005, *ApJ*, 635, 386 (Paper II)
- Yao, Y., & Wang, Q. D. 2005, *ApJ*, 624, 751 (Paper I)
- Young, P. R. 2005, *A&A* submitted, *astro-ph/0510264*